An analog experiment of the parametric instability

R. Berthet,[a] A. Petrosyan,[b] and B. Roman[c]
Laboratoire de Physique, UMR CNRS 5672, Ecole Normale Supérieure de Lyon, 46 Allée d'Italie, 69364 Lyon Cedex 07, France

(Received 11 February 2000; accepted 7 March 2002)

We show how a simple electronic parametric oscillator can be used to exhibit both supercritical and subcritical bifurcations to a subharmonic oscillatory state as the pump frequency is varied, and study the scaling behavior of the oscillation amplitude in the vicinity of the tricritical point. © *2002 American Association of Physics Teachers.*

[DOI: 10.1119/1.1477428]

I. INTRODUCTION

Parametric amplifiers and oscillators have been widely studied in electronics and optics. For instance, parametric amplification has been used to achieve low-noise amplification in electronic systems.[1] Many other applications, from particle traps to the stability of a floating body,[2] show the great importance of parametric resonance as was pointed out by Brillouin at the end of the 19th century.[3] More recently, the frequency and phase selectivity of parametric resonance has been used to implement noise-squeezing devices.[4] Canonical examples of parametric resonance are the stabilization of an inverted pendulum and the first resonance of the Melde string.[2,5,6] Another example leading to parametric oscillations is the swing on which most people have played. As pointed out by Case,[7,8] a pumped swing is both a driven oscillator and a parametric oscillator. In the playground, the commonly chosen motion corresponds to the driven oscillator. Nevertheless, parametric pumping is also possible and can occur for large oscillation angles.[7] Such oscillations can be easily studied experimentally using a simple pendulum with an oscillating support.[5,9,10]

Parametric instability also occurs when a tank containing a liquid is vertically vibrated: one then observes standing waves on the free surface.[11] This parametric instability is called the Faraday instability. The physical situation is more complex because of the great number of degrees of freedom in the system leading to the generation of complex patterns on the surface.[12] The study of parametric surface waves has led to a large number of theoretical and experimental studies.[13–16] In the simple case of an incompressible, irrotational, and inviscid fluid, Benjamin and Ursell[17] showed that, in the linear approximation, each mode ζ_k (of wave vector $\mathbf{k}$) of the surface deformation is governed by a Mathieu equation,

$$\ddot{\zeta}_k+\omega_0^2(k)[1+F\sin(\omega_e t)]\zeta_k=0, \tag{1}$$

where the dot indicates differentiation with respect to the time t, ω_e is the external forcing pulsation, and F is directly related to the amplitude of the vibration acceleration relative to the acceleration of gravity. The presence of a small viscous dissipation can be taken into account by including a phenomenological damping term $2\lambda\dot{\zeta}$ in Eq. (1), leading to

$$\ddot{\zeta}_k+2\lambda\dot{\zeta}_k+\omega_0^2(k)[1+F\sin(\omega_e t)]\zeta_k=0. \tag{2}$$

Other terms due to viscous dissipation are present in general.

Recently, Pritchett and Kim proposed a simple system to observe Faraday instabilities.[18] We propose here an alternative way to study parametric instabilities by doing an analog experiment that models the Mathieu equation in Eq. (2). As mentioned in Ref. 19, our proposed experiment is easy to understand conceptually and has several advantages, including fast data acquisition. It also allows students to explore the behavior of a driven oscillator and to understand the concepts of supercritical and subcritical bifurcations.

The experiments involve two control parameters: the forcing amplitude F and the forcing pulsation ω_e. Varying these two parameters allows us to study the threshold of the instability for different driving frequencies and to explore the Mathieu tongue of the bifurcation. We also study the nonlinear dependence of the oscillation amplitude on F.

After a brief review of the theoretical results for the parametric oscillator, we present our analog electronic system in Sec. III. Section IV discusses our results and the significance of our system for studying parametric resonance. In Sec. V we discuss future applications of our experiment to the study of noise-induced phase transitions.

II. PARAMETRIC RESONANCE

A system is subjected to a parametric forcing if one of its parameters is temporally modulated. We consider a simple pendulum of length l subject to a linear damping force and to the acceleration of gravity g. Its support oscillates vertically with a frequency f_e and a forcing amplitude F. As mentioned in Sec. I, this system leads to a canonical example of a parametric instability.[9,10,20] The evolution of the pendulum angle θ with respect to the vertical is governed by the Mathieu equation (2) with a nonlinear term,

$$\frac{d^2\theta}{dt^2}+2\lambda'\frac{d\theta}{dt}+\omega_0^2[1+F\sin(\omega_e t)]\sin\theta=0 \tag{3}$$

with $\lambda'>0$, $\omega_0^2=g/l$, and $\omega_e=2\pi f_e$.

In the undamped case ($\lambda'=0$), when $F\to 0$, the parametric resonance occurs when $\omega_e/\omega_0=2/p$, where p is an integer. The most unstable oscillation corresponds to $p=1$, that is, $\omega_e=2\omega_0$.[20] In the following, we investigate only this case.

For small oscillations, Eq. (3) can be reduced to

$$\frac{d^2\theta}{d\tau^2}+2\lambda\frac{d\theta}{d\tau}+\left[1+4\mu\sin\left(\frac{\omega_e}{\omega_0}\tau\right)\right](\theta-\gamma\theta^3)\simeq 0, \tag{4}$$

where $\tau=\omega_0 t$, $\lambda=\lambda'/\omega_0$, $\mu=F/4$, and $\gamma=1/6$ for a pendulum. When λ, μ, and the detuning parameter $\nu=2(\omega_0^2/\omega_e^2-1/4)$ have the same order of magnitude ε ($\varepsilon\ll 1$), we can

use the method of multiple time scales to analyze Eq. (4). We use two time scales, τ and $T=\varepsilon\tau$, and expand the angle θ as

$$\theta(\tau)=\sqrt{\varepsilon}[\,\theta_0(\tau,T)+\sqrt{\varepsilon}\,\theta_1(\tau,T)+\varepsilon\,\theta_2(\tau,T)+\cdots]. \quad (5)$$

After substituting this expansion in Eq. (4) and collecting terms of the same order in ε, we obtain to zeroth order,

$$\frac{d^2\theta_0}{d\tau^2}+\theta_0=0, \quad (6)$$

which has the solution

$$\theta_0=X(T)e^{i\omega_0 t}+\text{complex conjugate}, \quad (7)$$

where the amplitude $X(T)$ is a complex function of T. The first-order equation has the same form and its solution only modifies $X(T)$. The second-order equation is

$$\frac{d^2\theta_2}{d\tau^2}+\theta_2=G\left[\,\theta_0,\mu\theta_0\sin\left(\frac{\omega_e}{\omega_0}\tau\right)\right]. \quad (8)$$

To avoid a secular growth of θ_2, the source term G of Eq. (8) must not include terms proportional to $\exp i(\omega_0)t$. If we use the zeroth-order solution (7), and the relation $\omega_e/\omega_0=2-4\nu$, this condition yields

$$\frac{dX}{dT}=(-\lambda+i\nu)X+\mu\overline{X}e^{-4i\nu T}-i\frac{3\gamma}{2}|X|^2X, \quad (9)$$

where $\overline{X}$ is the complex conjugate of X. Equation (9) can be expressed in a frame of reference rotating with frequency $f_e/2$ as[21]

$$\frac{dA}{dT}=(-\lambda+i\nu)A+\mu\overline{A}-i\frac{3\gamma}{2}|A|^2A, \quad (10)$$

where we have let $X=Ae^{-2i\nu T}$. The first term on the right-hand side of Eq. (10) is simply related to the damping of the pendulum. The two contributions with purely imaginary coefficients, $i(\nu-3\gamma|A|^2/2)A$, involve a rotation of A in the complex plane, and thus a detuning. This detuning depends in a nonlinear way on the oscillation amplitude $|A|$. The third term is proportional to $\overline{A}$ and represents the parametric forcing.

We can study both the linear and nonlinear stability of the equilibrium solution $\theta=0$. If we let $A=(x+iy)e^{\eta t}$, we find that the solution $A=0$ is linearly stable for $\eta<0$; otherwise, it is unstable. If we drop the nonlinear term $|A|^2A$ in Eq. (10), the solution $\theta=0$ is found to be linearly stable when μ is smaller than μ_c, where

$$\mu_c=\sqrt{\lambda^2+\nu^2}. \quad (11)$$

The nonlinear analysis shows that for $\mu>\mu_c$ $(F>F_c)$, oscillations of frequency $f_e/2$ appear to grow in amplitude until $dA/dT=0$. When this steady state is reached, the amplitude $|A|$ can be obtained from Eq. (10) by setting $dA/dT=0$ and writing $A=Re^{i\theta}$. By setting the real and imaginary parts of Eq. (10) equal to zero and using $\cos^2(2\theta)+\sin^2(2\theta)=1$, $|A|=R$ is determined by the relation

$$|A|^2=\frac{2}{3\gamma}(\nu\mp\sqrt{\mu^2-\lambda^2}). \quad (12)$$

We can discuss the nature of the solutions in terms of bifurcations (see also Fig. 1).[21,22]

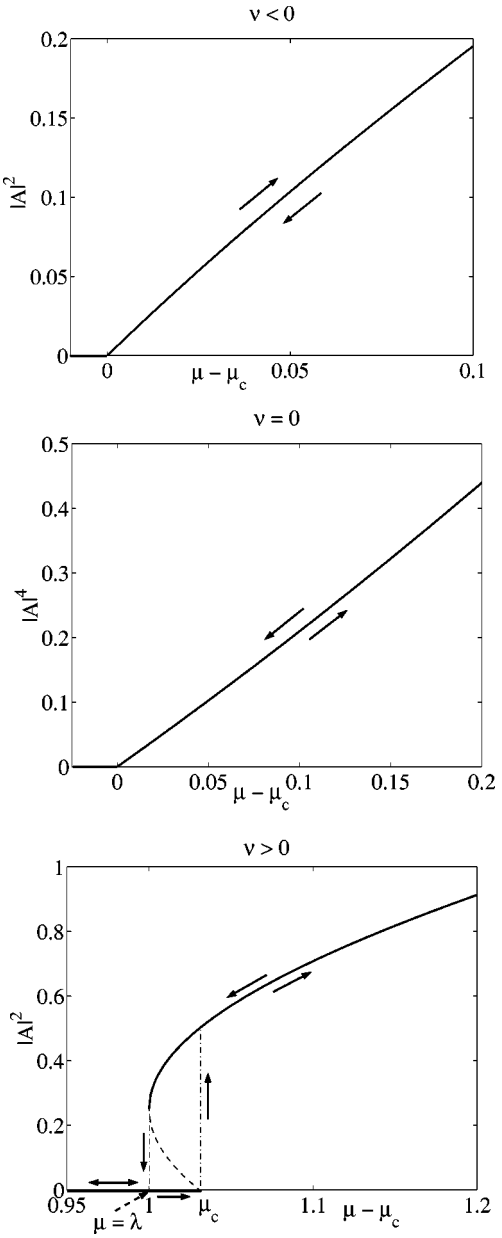

Fig. 1. Bifurcation diagrams for the parametric oscillator: supercritical case ($\nu<0$), tricritical case ($\nu=0$), and subcritical case ($\nu>0$). The arrows indicate the pendulum amplitude evolution when the forcing amplitude is increasing or decreasing.

(1) For $\nu>0$ $(f_e<2f_0)$, the bifurcation is subcritical. There are two solutions such that $|A|\neq 0$ for $\lambda\leqslant\mu\leqslant\mu_c$, and one solution $|A|\neq 0$ for $\mu>\mu_c$.
(2) For $\nu<0$ $(f_e>2f_0)$, the bifurcation is supercritical, and there is only one solution, $|A|\neq 0$, with two opposite phases. Near the threshold μ_c, Eq. (12) leads to the scaling $|A|\propto(\mu-\mu_c)^{1/2}$ and $|A|^2\propto(\mu-\mu_c)$.
(3) For $\nu=0$, there is a tricritical point (the bifurcation is subcritical for $\nu\gtrsim 0$ and supercritical for $\nu\lesssim 0$). We find that $|A|\propto(\mu-\mu_c)^{1/4}$ and $|A|^4\propto(\mu-\mu_c)$ near the threshold.

We see that we expect a crossover between the two types of behavior when $\nu\lesssim 0$. This point will be discussed in detail in Sec. IV.

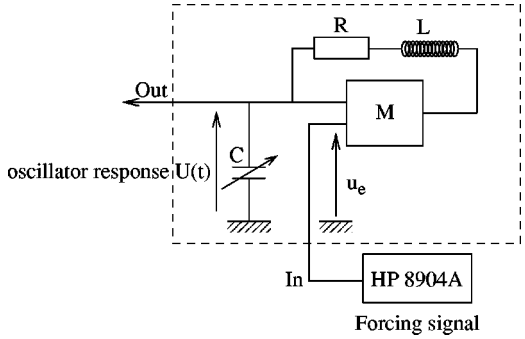

Fig. 2. Electronic analog of the Mathieu equation.

III. THE ANALOG MODEL

A. Experimental setup

As mentioned in Sec. I, we will develop an analog model of the parametric instability. In fact, the Mathieu equation, Eq. (3), leads to the amplitude in Eq. (12), which is analogous to the one derived in the Faraday problem in the limit of small viscosity.[23] Our electronic device is shown in Figs. 2 and 3. M is an AD633 multiplier; its output voltage, s, is proportional to the product of the two input voltages, e_1 and e_2: $s=ke_1\times e_2$. C is a capacitor with a voltage-dependent capacity made with variable capacitance diodes (varicaps) BB909A. As mentioned in Ref. 5, these diodes introduce some nonlinearities in contrast to the circuit proposed in Ref. 24 where no nonlinear component is present. To avoid electromagnetic perturbations, the electronic oscillator is enclosed in a metallic container which serves as a Faraday cage.

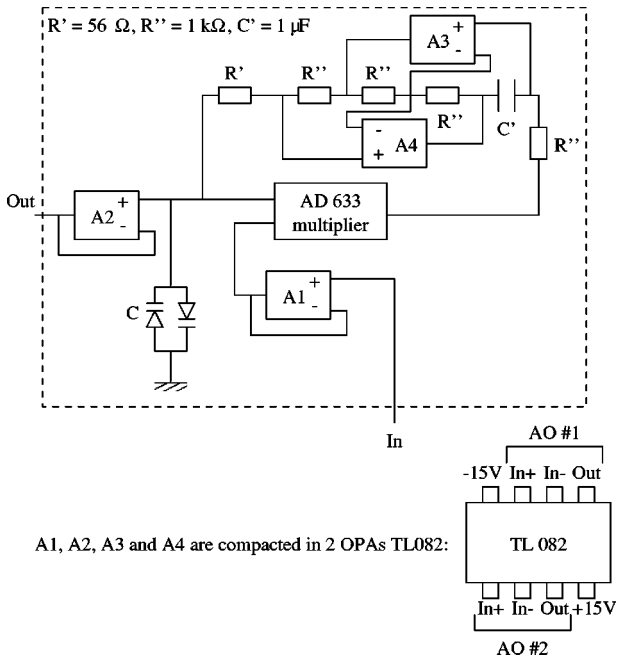

Fig. 3. Details of the electronic system inside the dashed box in Fig. 2, between points A and B. Operational amplifiers A_1, A_2, A_3, and A_4 are compacted using two dipole OPAs TL082, but can be compacted using a quadrupole OPA TL084. A single OPA TL081 can also be used. A_1 and A_2 are used in building followers (Ref. 27); A_3 and A_4 are used for the gyrator filter.

The electronic system is forced by a periodic voltage $u_e(t)=u_0\sin(\omega_e t)$. We can use Kirchhoff's voltage law[1] and the property of the multiplier to find that the charge q of the capacitance C is governed by (see Fig. 2)

$$\frac{d^2q}{dt^2}+\frac{R}{L}\frac{dq}{dt}+\frac{q}{LC}[1+ku_0\sin(\omega_e t)]=0, \tag{13}$$

where k is the gain of the multiplier ($k=\frac{1}{10}V$ in our case). The capacitance C depends on the charge q, but the use of a pair of oppositely polarized varicaps leads to the symmetry $q\rightarrow -q$ of the function $C(q)$. Hence, we can write[5,25]

$$C\simeq C_0(1+\gamma q^2)\quad(\gamma>0) \tag{14}$$

and Eq. (13) becomes

$$\ddot{q}+2\lambda'\dot{q}+\omega_0^2[1+F\sin(\omega_e t)](q-\gamma q^3)\simeq 0, \tag{15}$$

with $2\lambda'=R/L$, $\omega_0^2=1/LC_0$, and $F=ku_0$. If we use the dimensionless variables $\tau=\omega_0 t$, $\lambda=\lambda'/\omega_0$, and $\mu=F/4$, we can write Eq. (15) as

$$\frac{d^2q}{d\tau^2}+2\lambda\frac{dq}{d\tau}+\left[1+4\mu\sin\left(\frac{\omega_e}{\omega_0}\tau\right)\right](q-\gamma q^3)\simeq 0. \tag{16}$$

Equation (16) is identical to Eq. (3) and we can expect experimental results for the charge amplitude similar to those described in Sec. II for the pendulum amplitude.

We used a 1-H inductance, and measured the resonance frequency of the RLC circuit to be $f_0\simeq 6.812$ kHz so that $C_0\simeq 546$ pF. For $\omega_e=2\omega_0$, the threshold is simply determined by the relation $\mu_c=\lambda=R/(2L\omega_0)$. Thus, the global resistance of the circuit is $R\simeq 555\ \Omega$, and the quality factor of the RLC circuit is $Q=L\omega_0/R\simeq 77$. As mentioned below, we are interested in the evolution of the voltage $U\simeq q/C_0$, the analog of the pendulum angle θ in Sec. II. We thus utilize a digital synthesizer HP8904A and a signal analyzer HP35670A (see Fig. 2) to calculate, via a real-time averaged fast Fourier transform, the voltage amplitude $|A|$, defined by

$$U(t)=Ae^{i\omega_e t/2}+\text{complex conjugate}. \tag{17}$$

After interfacing the experimental setup using LABVIEW, we can directly record the control parameters u_0 and f_e, and the voltage amplitude $|A|$.

B. Technical comments

Despite the simplicity of our electronic scheme, two technical points must be stressed. First, the 1-H inductance is realized using a gyrator filter,[26] which gives a large inductance value independent of the frequency with no resistance and a small scale size.

The other point is linked to the purpose of the experiment. In an educational context, the circuit can be used as we have discussed because highly reproducible results are not absolutely essential, and the most important objective is that students understand the physical concepts of nonlinearity and parametric resonance. However, for quantitative experiments, highly reproducible results are necessary. Thus, even with good quality electronic components (low noise and great precision), temperature effects should not be underestimated because diurnal temperature variations can change the instability threshold by a factor of 2 or so. We have added a thermal regulation system (the container is in contact with circulating water at fixed temperature) to control the tem-

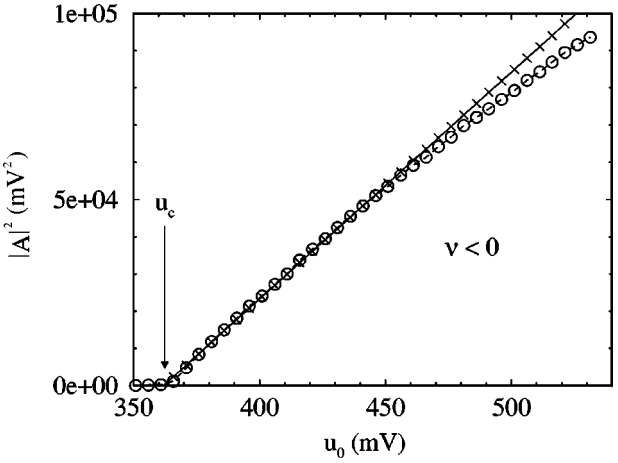

Fig. 4. Dependence of the pendulum amplitude $|A|$ on the driving voltage $u_0(\propto\mu)$ for $f_e=13.700$ kHz ($\nu\simeq-237$ s^{-1}). ($\bigcirc$) corresponds to the experimental data for $|A|^2$ and ($\times$) to the linear fit to the data near the threshold of the parametric instability.

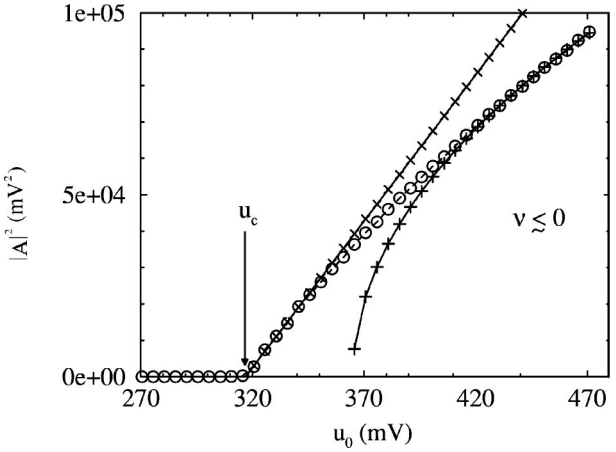

Fig. 6. Dependence of the pendulum amplitude $|A|$ on the driving voltage $u_0(\propto\mu)$ for $f_e=13.675$ kHz ($\nu\simeq-159$ s^{-1}). ($\bigcirc$) corresponds to the experimental data for $|A|^2$, ($\times$) to the linear fit to the data near the threshold of the instability, and ($+$) to the linear fit of $|A|^4$ with u_0 far from the threshold to illustrate the crossover phenomenon.

perature of the system and ensure reproducibility of our results. Our tests show that with this regulation system, our measurements are reproducible by $\pm5\%$. For all the results presented in Sec. IV, the measurement errors are less than 1% for u_0 and f_e and within 5% for $|A|$.

IV. RESULTS AND DISCUSSION

Our first observations consist of choosing a frequency f_e [that is, fixing ν in Eq. (10)] and varying the forcing amplitude u_0 [μ in Eq. (10)]. Thus, we can study the evolution of the charge q, or in a similar way, the evolution of the voltage $U=q/C\simeq q/C_0$, and look for the threshold of the parametric instability.

In Figs. 4–7, we present the evolution of $|A|$ to some power with u_0 so that we can make a direct comparison with the theoretical results presented in Sec. II: u_0 is the analog of μ in Eq. (10). We immediately observe that the experimental results are difficult to interpret in terms of bifurcation. To help our understanding, we have made some fits of the experimental data near the threshold of the instability for three values of the detuning parameter ν.

(1) For $\nu<0$ (Fig. 4), we see that increasing the pump voltage u_0 starting from below the threshold u_c [$\mu_c=\sqrt{\lambda^2+\nu^2}$ in Eq. (12)] or decreasing u_0 starting from above the threshold leads to the same value of $|A|$. Figure 4 shows good agreement between the theoretical predictions and our data near the threshold: $|A|^2$ scales like (u_0-u_c). For the largest forcing amplitudes, we are far from the threshold and the oscillator enters the crossover region mentioned in Sec. II (see details below and Fig. 6) as long as no other nonlinear effects occur.

(2) For $\nu\simeq0$ (Fig. 5), our results are also in good agreement with the predictions, that is, $|A|^4$ scales like (u_0-u_c), except for values of the forcing amplitude near u_c. In this region, the oscillator is very sensitive to both amplitude and detuning perturbations of the pump. Therefore, we can expect a lack of accuracy in the measurement of the amplitude. The data presented in Fig. 6 show a typical example of the crossover region mentioned at the end of Sec. II. Near the threshold, the system is very sensitive to the detuning. Thus, the oscillator's amplitude has the same be-

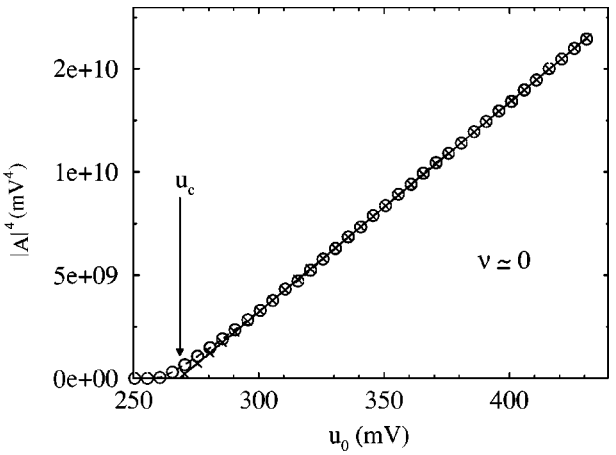

Fig. 5. Dependence of the pendulum amplitude $|A|$ on the driving voltage $u_0(\propto\mu)$ for $f_e=13.625$ kHz$\simeq2\,f_0$ ($\nu\simeq-3$ s^{-1}). ($\bigcirc$) corresponds to the experimental data for $|A|^4$ and ($\times$) to the linear fit of the data near the threshold of the instability.

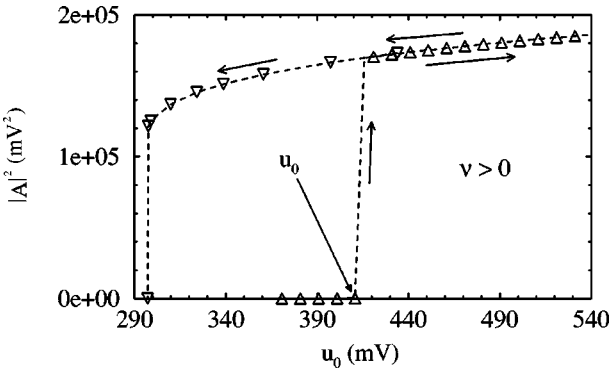

Fig. 7. Dependence of $|A|^2$ on the driving voltage $u_0(\propto\mu)$ for $f_e=13.500$ kHz ($\nu\simeq395$ s^{-1}): ($\triangle$) for increasing u_0 and ($\triangledown$) for decreasing u_0.

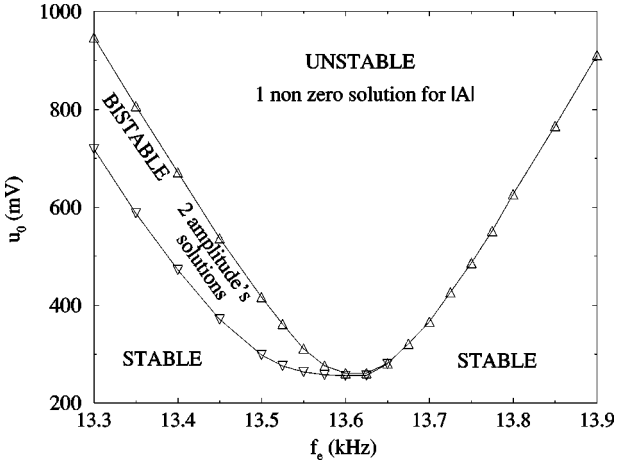

Fig. 8. Experimental tongue for the parametric instability: (△) for increasing $u_0(\propto\mu)$ and (▽) for decreasing u_0.

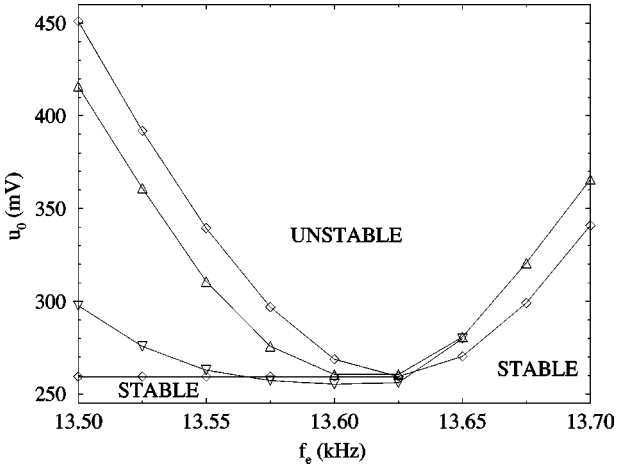

Fig. 9. Comparison of the theoretical tongue (◇) with our results: (△) for increasing $u_0(\propto\mu)$ and (▽) for decreasing u_0.

havior as for a supercritical bifurcation, $|A|\propto(u_0-u_c)^{1/2}$. When the pump amplitude increases, the system is less sensitive to the detuning and acts as in the case of zero detuning. So, as long as no other nonlinearities occur, $|A|\propto(u_0-u_c)^{1/4}$. We can also observe by comparing Figs. 4 and 6 that the bigger the detuning, the larger the supercritical transition region, in agreement with the explanation given above.

(3) For $\nu>0$ corresponding to a subcritical transition, increasing u_0 starting from below the threshold or decreasing u_0 starting above the threshold leads to two different evolutions of the amplitude $|A|$ with u_0, as shown in Fig. 7. This behavior is typical of a subcritical bifurcation. It is important to notice that the forcing amplitude should be decreased keeping the phase locked with that of the oscillator. If this phase lock-in is not realized, the system jumps to the stable state ($|A|=0$) for $\lambda\leqslant u_0\leqslant u_c$. This phase lock-in is realized by changing the amplitude with a potential divider (full resistance $R=10\ \mathrm{k}\Omega$) between the synthesizer and the circuit input (point A in Fig. 2), instead of directly varying the synthesizer output voltage starting from $u_{0i}>u_c$. This lock-in ensures the stability of the phase during the decreasing part of the measurements.

We see that our measurements are in good agreement with the theoretical prediction of the bifurcation diagrams of the parametric oscillator. We now change both the forcing amplitude u_0 and the pump frequency f_e in order to explore the (f_e,u_0) plane. The corresponding Mathieu tongue (the critical forcing amplitude u_c versus the forcing frequency) is presented in Fig. 8 for the entire domain of the measurements. The (f_e,u_0) plane is divided into three regions. For (f_e,u_0) above all the curves, the oscillator is unstable; for (f_e,u_0) below all the curves, the oscillator is stable, and between the two curves the oscillator is bistable. In the latter region, the system can change between two states, oscillations or steady state $|A|=0$, for finite amplitude perturbations, in contrast with the two other regions of the graph.

For comparison with the theoretical prediction $\mu_c=\sqrt{\lambda^2+\nu^2}$, we have shown in Fig. 9 the tongue in the region where $\lambda\sim\nu\sim\mu$, which in terms of frequencies is $13.500\ \mathrm{kHz}\lesssim f_e\lesssim 13.750\ \mathrm{kHz}$. We first remark that the border of the bistable region is not a horizontal line, which is probably due to the presence of a nonlinear component in the damping term and the inaccuracy in the measurements when the forcing amplitude decreases for $f_e<2f_0$.

In our experiments, the amplitude equation has the form in Eq. (10) with the parameters of Eq. (16):

$$\frac{dA}{dT}=(-\lambda+i\nu)A+\mu\overline{A}-i\frac{3\gamma}{2}|A|^2A, \tag{18}$$

with $\lambda=R/(2L\omega_0)$ and $\mu=u_0/40$. So, the linear stability of the solution is (u_0 in V)

$$u_0=\frac{40}{\omega_0}\sqrt{\left(\frac{R}{2L}\right)^2+\omega_0^2\nu^2}.$$

We can directly compare our system with the parametric system studied in Sec. II. Figure 9 shows quite good agreement between our system and an ideal parametric pendulum—the errors are less than 10%. We believe that the biggest part of this error is due to an inaccuracy in the determination of the RLC resonance frequency f_0.

Finally, we present a measurement to determine the nonlinear coefficient γ. We use the relation (12) in the supercritical case $\nu<0$:

$$|A|^2=\frac{2}{3\gamma}(\nu+\sqrt{\mu^2-\lambda^2}). \tag{19}$$

Near the threshold, we can derive, for $\nu<0$,

$$|A|^2=\frac{-2\mu_c}{3\gamma\nu}(\mu-\mu_c), \tag{20}$$

which for our system is

$$|A|^2=\left(\frac{-\mu_c\,\omega_0}{60\gamma\nu}\right)u_0+\frac{2\mu_c^2}{3\gamma\nu}. \tag{21}$$

The value of γ is thus determined by choosing a large detuning value (see Fig. 10) to ensure a scaling behavior in $|A|^2\propto(u_0-u_c)$. A linear fit of the data gives $\gamma\simeq 3.81\times10^{-2}\,C^{-2}$ using the slope and $\gamma\simeq 3.53\times10^{-2}\,C^{-2}$ using the intersection with the y axis. Hence, we estimate $\gamma\simeq 1/27\,C^{-2}$, and Eq. (16) for the oscillator takes the final form

$$\ddot{q}+2\lambda\dot{q}+\omega_0^2[1+F\sin(\omega_e t)](q-q^3/27)\simeq 0. \tag{22}$$

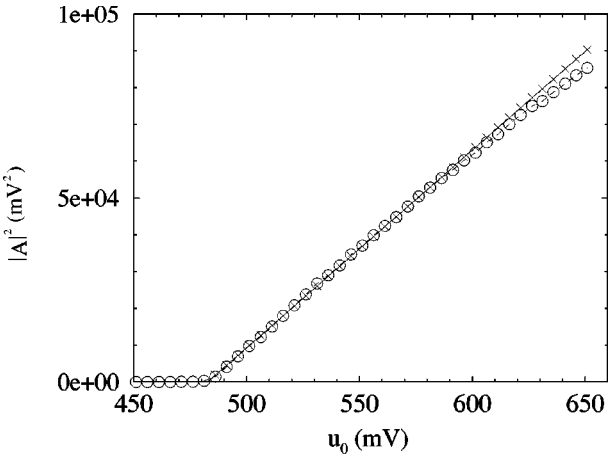

Fig. 10. Dependence of $|A|^2$ on the driving voltage $u_0(\propto\mu)$ for $f_e = 13.750$ kHz ($\nu \simeq -390$ s^{-1}): the linear fit is made on the linear part of the curve (490 mV$\leqslant u_0 \leqslant$600 mV) to avoid crossover effects. ($\bigcirc$) corresponds to the experimental data and ($\times$) to the linear fit.

Starting from Eq. (22), we note that scaling q allows us to find the parametric pendulum Eq. (4). That is, if we let $q = \alpha\,\theta$, we find

$$\ddot{\theta} + 2\lambda\,\dot{\theta} + \omega_0^2[1 + F\sin(\omega_e t)](\theta - (\alpha^2/27)\,\theta^3) \simeq 0, \quad (23)$$

which is exactly Eq. (4) for $\alpha = \sqrt{27/6}$.

V. CONCLUSION

We have presented an experimental study of parametric resonance, which can be used to describe various nonlinear phenomena qualitatively and to obtain the bifurcation diagrams quantitatively. It is based on an electronic circuit and is easy to use. We have shown that it is a good simulation of parametric phenomena, and our results are in good agreement with theoretical predictions. In particular, it may be used to study the influence of pump noise on the instability's threshold and amplitude.

ACKNOWLEDGMENTS

We wish to thank S. Fauve for helpful discussions and for taking time to read the draft of this paper. We acknowledge support from Contract No. INTAS 97-1672.

[a]Present address: LPS, UMR CNRS 8550, École Normale Supérieure, 24 Rue Lhomond, 75231 Paris Cedex 05, France; electronic mail: remy.berthet@lps.ens.fr

[b]Permanent address: Yerevan St. University, 1, A. Manoogian, Yerevan, Armenia.

[c]Present address: IRPHE, UMR CNRS 6594, Universités Aix-Marseille I & II, Centre Saint Jérôme, S. 252, 13397 Marseille Cedex 20, France.

[1]P. Horowitz and W. Hill, *The Art of Electronics* (Cambridge U.P., Cambridge, 1989), 2nd ed., p. 903.

[2]L. Ruby, "Applications of the Mathieu equation," Am. J. Phys. **64**, 39–44 (1996).

[3]M. Brillouin, "Théorie d'un alternateur auto-excitateur," L'Éclairage Électrique **XI-15**, 49–59 (1897).

[4]D. Rugar and P. Grütter, "Mechanical parametric amplification and thermomechanical noise squeezing," Phys. Rev. Lett. **67**, 699–702 (1991).

[5]L. Falk, "Student experiments on parametric resonance," Am. J. Phys. **47**, 325–328 (1979).

[6]E. D. Yorke, "Square-wave model for a pendulum with oscillating suspension," Am. J. Phys. **46**, 285–288 (1978).

[7]W. Case, "The pumping of a swing from the seated position," Am. J. Phys. **58**, 463–467 (1990).

[8]W. Case, "The pumping of a swing from the standing position," Am. J. Phys. **64**, 215–220 (1996).

[9]W. Case, "Parametric instability: An elementary demonstration and discussion," Am. J. Phys. **48**, 218–221 (1980).

[10]F. L. Curzon, A. L. H. Loke, M. E. Lefrançois, and K. E. Novik, "Parametric instability of a pendulum," Am. J. Phys. **63**, 132–136 (1995).

[11]M. Faraday, "On the forms and states assumed by fluids in contact with vibrating elastic surfaces," Philos. Trans. R. Soc. London **52**, 319–340 (1831).

[12]W. S. Edwards and S. Fauve, "Parametrically excited quasicrystalline surface waves," Phys. Rev. E **47**, 788–791 (1993).

[13]K. Kumar, "Linear theory of Faraday instability in viscous liquids," Proc. R. Soc. London, Ser. A **452**, 1113–1126 (1996).

[14]J. Bechhoefer, V. Ego, S. Manneville, and B. Johnson, "An experimental study of the onset of the parametrically pumped surface waves in viscous fluids," J. Fluid Mech. **288**, 325–350 (1995).

[15]S. Douady, Ph.D. thesis, ENS-Lyon, 1989 (unpublished).

[16]S. Fauve, K. Kumar, C. Laroche, D. Beysens, and Y. Garrabos, "Parametric instability of a liquid-vapor interface close to the critical point," Phys. Rev. Lett. **68**, 3160–3163 (1992).

[17]T. B. Benjamin and F. Ursell, "The stability of the plane free surface of a liquid in vertical periodic motion," Proc. R. Soc. London, Ser. A **225**, 505–515 (1954).

[18]T. Pritchett and J. K. Kim, "A low-cost apparatus for the production of surface wave patterns in a vertically oscillating fluid," Am. J. Phys. **66**, 830–833 (1998).

[19]D. G. Luchinsky, P. V. E. McClintock, and M. I. Dykman, "Analogue studies of non-linear systems," Rep. Prog. Phys. **61**, 889–997 (1998).

[20]L. Landau and E. Lifschitz, *Mechanics* (Pergamon, London, 1960), Sec. 27.

[21]S. Fauve, in "Pattern forming instabilities," in *Woods Hole GFD Summer School Technical Report*, 1991 and in *Hydrodynamics and Non-Linear Instabilities*, edited by C. Godrèche and P. Manneville (Cambridge U.P., Cambridge, 1998), Chap. 4.

[22]J. Guckenheimer and P. Holmes, *Nonlinear Oscillations, Dynamical Systems and Bifurcations of Vector Fields*, Applied Mathematical Sciences Vol. 42 (Springer, New York, 1983), p. 149.

[23]S. Fauve, "Waves on interfaces," in *Free Surface Flows*, International Centre for Mechanical Sciences Courses and Lectures, No. 391 (Springer-Wien, New York, 1998).

[24]F. X. Bally and P. Boissé, "Un modèle électronique simple et exact de l'oscillateur paramétrique," Bulletin de l'Union des Physicens **747**, 1267–1276 (1992).

[25]Technical documentation on varicap BB909A, Philips Semiconductors.

[26]Reference 1, Sec. 5.10.

[27]Reference 1, Sec. 4.06.